

Signal Processing for Passive Radar Using OFDM Waveforms

Christian R. Berger, *Member, IEEE*, Bruno Demissie, *Member, IEEE*, Jörg Heckenbach, Peter Willett, *Fellow, IEEE*, and Shengli Zhou, *Member, IEEE*

Abstract—Passive radar is a concept where illuminators of opportunity are used in a multi-static radar setup. New digital signals, like Digital Audio/Video Broadcast (DAB/DVB), are excellent candidates for this scheme, as they are widely available, can be easily decoded to acquire the noise-free signal, and employ orthogonal frequency division multiplex (OFDM). Multicarrier transmission schemes like OFDM use block channel equalization in the frequency domain, efficiently implemented as a fast Fourier transform (FFT), and these channel estimates can directly be used to identify targets based on Fourier analysis across subsequent blocks. In this paper, we derive the exact matched filter formulation for passive radar using OFDM waveforms. We then show that the current approach using Fourier analysis across block channel estimates is equivalent to the matched filter, based on a piecewise constant assumption on the Doppler induced phase rotation in the time domain. We next present high-resolution algorithms based on the same assumption: first we implement MUSIC as a two-dimensional spectral estimator using spatial smoothing; second we use the new concept of compressed sensing to identify targets. We compare the new algorithms and the current approach using numerical simulation and experimental data recorded from a DAB network in Germany.

Index Terms—Multi-static radar, radar processing, compressed sensing, sparse estimation, MUSIC, subspace algorithms.

I. INTRODUCTION

A. Passive Radar: Motivation & Challenges

In passive radar, illuminators of opportunity are used to detect and locate airborne targets. This is essentially the same as a bi-static radar setup, as sender and receiver are not co-located, and time difference of arrival (TDoA) measurements

Manuscript submitted February 2, 2009, revised May 10, 2009, accepted October 1, 2009. This work was supported by ONR grant N00014-07-1-0429. Parts of this work were presented at the International Conference on Information Fusion in Cologne, Germany, Jul. 2008, and at the Asilomar Conference on Signals, Systems, and Computers in Monterey, CA, Oct. 2008.

Copyright ©2008 IEEE. Personal use of this material is permitted. However, permission to use this material for any other purposes must be obtained from the IEEE by sending a request to pubs-permissions@ieee.org.

C. Berger was with the Department of Electrical and Computer Engineering, University of Connecticut. He is now with the Department of Electrical and Computer Engineering, Carnegie Mellon University, Pittsburgh, PA 15213 USA (e-mail: crberger@ece.cmu.edu).

B. Demissie is with the Fraunhofer Institute for Communication, Information Processing and Ergonomics FKIE, Neuenahrer Str. 20, 53343 Wachtberg, Germany (email: bruno.demissie@fkie.fraunhofer.de).

J. Heckenbach is with the Fraunhofer Institute for High Frequency Physics and Radar Techniques FHR, Neuenahrer Str. 20, 53343 Wachtberg, Germany (email: joerg.heckenbach@fhr.fraunhofer.de).

P. Willett, and S. Zhou are with the Department of Electrical and Computer Engineering, University of Connecticut, 371 Fairfield Way U-2157, Storrs, Connecticut 06269, USA (email: {willett, shengli}@engr.uconn.edu).

Digital Object Identifier 00.0000/JSTSP.2009.000000

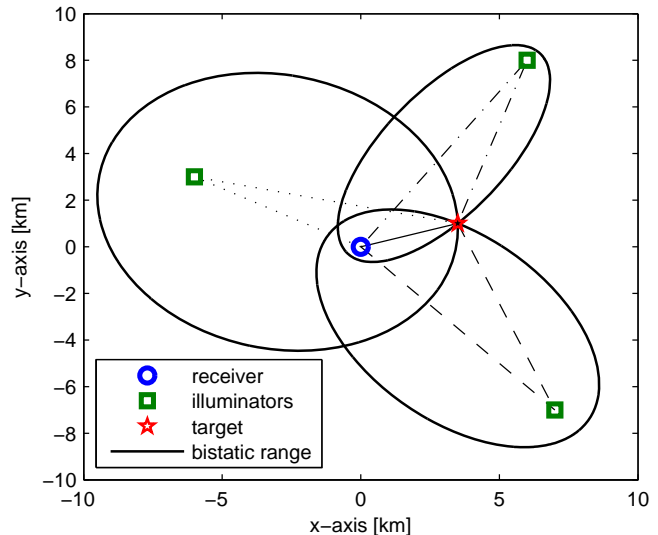


Fig. 1. In passive radar, illuminators of opportunity are used in a multi-static setup; weak target signatures can be extracted from the dominating directly received radio/television signal based on their Doppler frequency, rendering bi-static range and range-rate information.

localize targets on ellipses around the sender-receiver axis, c.f. Fig. 1 and [1]. It is the differences, though, that make passive radar attractive; i) as the illuminators are not part of the radar system, its presence is virtually undetectable; ii) illuminators of opportunity are often radio and TV stations, broadcasting in the VHF/UHF frequency bands otherwise not available to radar applications. The first point, in conjunction with the bi-static setup, makes it impossible for targets to know if they have been detected, while the operation in the radio/TV VHF/UHF frequency bands needs no frequency allocation, gives frequency diversity, and can help to detect low-flying targets beyond the horizon [2], [3].

Challenges connected to implementing a passive radar system are mostly due to using broadcast signals, which are not under control, for illumination. Therefore the transmitted signals are not known a priori, which means that a regular matched filter based receiver cannot be implemented easily. Second, although broadcast antennas are sectorized at times, since broadcast signals have to cover a broad area the transmit antennas are approximately isotropic and there is no significant transmitter gain. This can lead to constraints on the achievable range of a passive radar, if the transmit signal does not belong

to a high power regional broadcast station. Last, since the illumination is continuous, there is no easy way to separate the direct signal from reflections off targets in the time domain, as is typically done in bi-static settings.

B. Current State-of-the-Art

First systems working with analog broadcast (TV/FM) used the direct signal as a noisy template to implement an approximate matched filter [4]–[8]. Newly available digital broadcast systems give passive radar receivers the unique opportunity to perfectly reconstruct the transmitted signal after successful demodulation and forward error correction (FEC) coding [9]–[14]. A big challenge is also to excise the direct signal. Also, the received signal has a dynamic range of easily 100 dB between direct signal and targets, due to possibly small target radar-cross-section (RCS) and large coverage area, which cannot be handled by analog-to-digital converters. This makes additional analog pre-compensation of the direct signal necessary, e.g., in the form of null-steering or directional antennas, see [7].

A current state-of-the-art system has the following structure, see e.g. [10],

- 1) The digital broadcast signal is decoded and perfectly reconstructed based on the direct signal.
- 2) Null steering attenuates the direct signal to the level of clutter, reducing the required dynamic range to below 70 dB.
- 3) The signal is divided into segments.
- 4) Matched filtering is performed efficiently in the frequency domain using the fast Fourier transform (FFT).
- 5) A second Fourier transform is executed across segments to separate low SNR targets from the dominant direct signal and clutter based on Doppler information.

The last three steps are illustrated in Fig. 2; the outputs of such a processing chain are bi-static range and range-rate, locating targets on ellipses around the transmitter/receiver axis; see Fig. 1. This implementation is especially applicable in digital multi-carrier broadcast systems, such as digital audio/video broadcast (DAB/DVB), as the transmit signal is specifically designed for frequency domain equalization.

Further challenges include target localization and tracking; as in the present system angle-of-arrival (AoA) information is often unreliable, localization has to be accomplished by finding the intersection of the ellipses from different transmitters. This highlights another unique feature of DAB/DVB, the operation in what is termed a “single frequency network” (SFN). This means that the same signal is transmitted by a network of broadcast stations in the same frequency band. For the purpose of target localization and tracking this delivers multiple “free” measurements per target within the same operating bandwidth. This offers the opportunity to gain diversity with respect to RCS fluctuations, but also poses an additional association problem, as it can not be determined which target echo originated from which transmitter. Suggested approaches include target tracking based on the probability hypotheses density (PHD) filter [15] and multiple hypotheses tracker (MHT) [16].

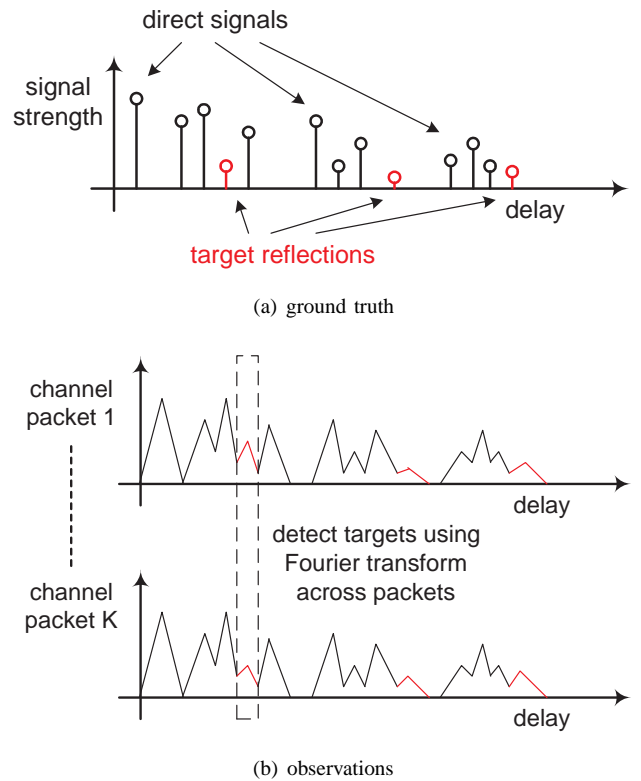


Fig. 2. The plot shows (a) target echoes within dense clutter; (b) time-domain channel estimates for subsequent OFDM packets; the targets can only be detected due to their non-zero range-rate, leading to phase changes over time that add constructively or destructively with stationary clutter.

C. Relationship to MIMO Radar

Although the prefix “MIMO” (multiple-input multiple-output) only specifies that multiple, spatially distributed transmitters and receivers are being used, MIMO radar is far from identical to the well-known multi-static radar. Since the MIMO principle was first successfully applied in wireless communications, MIMO radar has become a name for various advanced communications/signal-processing approaches being applied to radar signal processing and waveform design. One aspect of MIMO radar waveform design is that various transmitters can transmit independent waveforms – in sharp contrast to regular phased-array radars [17]. This promises improved parameter identifiability and more flexible beam pattern design. Another aspect is the inclusion of spatial diversity, for improved target detection and higher target position resolution, see [18].

Passive radar based on the new multicarrier DAB/DVB signals shares several of these trademarks, first there are multiple spatially distributed transmitters present operating on the same bandwidth (SFN concept), the transmitted waveforms are not traditional pulsed radar waveforms, and the receiver processing includes advanced digital signal processing to achieve high target resolution.

D. Our Work

We are interested in investigating passive radar using digital multicarrier modulated signals, as in the DAB scenario considered in [10], [11], [13], [14]. The signal is modulated

using orthogonal frequency division multiplex (OFDM), which is especially amenable to the FFT based approach outlined above. Our contributions are the following:

- 1) We derive the exact matched filter formulation for OFDM waveforms, which was not available before. We reveal that the practical approach, outlined in Section I-B, is equivalent to the matched filter, based on a piecewise constant approximation of the Doppler induced phase rotation in the time domain.
- 2) We investigate two signal processing schemes for passive radar: we show a link to two-dimensional direction finding and apply MUSIC; and we formulate the receiver as a sparse estimation problem to leverage the new compressed sensing framework to detect targets.
- 3) In addition to simulations, we test both the MUSIC and the compressed sensing based receivers on experimental data and point out practical implementation issues.

In a detailed simulation study we find that the piecewise constant approximation decreases the receiver performance by less than 3 dB for high Doppler targets. We also compare both receiver architectures against the current state-of-the-art approach, where we find that while more costly in complexity, the new algorithms offer advantages in target resolution and clutter suppression by removing sidelobes.

In the experimental data, we find that the biggest challenge is in handling the dominant clutter and direct signal, which can be easily 50 dB above the target signal strength. Both the conventional FFT processing based approach and the approach based on MUSIC need an additional step to remove the dominant clutter and direct signal, before these algorithms can work successfully. While in compressed sensing this is not necessary, we find that the lower complexity algorithm Orthogonal Matching Pursuit (OMP) [19], [20] cannot handle direct arrivals in the experimental data, but had to be replaced by the computationally more expensive Basis Pursuit (BP) [21]–[23].

The rest of this paper is organized as follows, in Section II we explain the signal model and derive the matched filter receiver, in Section III we show which approximations change the matched filter receiver into the FFT based receiver outlined above. Then in Section IV we show how to apply subspace algorithms, in Section V we leverage compressed sensing for improved performance, in Section VI we use numerical simulation, while in Section VII we take a look at experimental data, and conclude in Section VIII.

II. SIGNAL MODEL

A. Transmitted Signal

The Digital Audio Broadcast (DAB) standard [24], uses orthogonal frequency division multiplex (OFDM), which is a multicarrier modulation scheme, using N frequencies that are orthogonal given a rectangular window of length T at the receiver,

$$x_i(t) = \sum_{n=-N/2}^{N/2-1} s_i[n] e^{j2\pi n \Delta f t} q(t). \quad (1)$$

Accordingly each block carries N data symbols $s_i[n]$; the frequencies are orthogonal because the frequency spacing is $\Delta f = 1/T$, whereby the transmitted waveform is extended periodically by T_{cp} to maintain a cyclic convolution with the channel, i.e.,

$$q(t) = \begin{cases} 1 & t \in [-T_{cp}, T], \\ 0 & \text{otherwise.} \end{cases} \quad (2)$$

We define a symbol duration as $T' = T + T_{cp}$. The broadcast signal

$$x(t) = \sum_{i=-\infty}^{\infty} x_i(t - iT') \quad (3)$$

is continuous. The data symbols $s_i[n]$ vary with each block, but we assume they can always be decoded without error for our purposes¹. Some of the data symbols $s_i[n]$ might be deactivated for various reasons (protection of bandwidth edges, Doppler estimation, etc.) and, also, a complete Null symbol is inserted periodically for synchronization (all $s_i[n]$ are zero). The baseband signal is upconverted to the carrier frequency,

$$\tilde{x}(t) = \text{Re} \{ e^{j2\pi f_c t} x(t) \}. \quad (4)$$

B. Target/Channel Model

When a waveform is emitted by a transmitter, we expect to receive a direct arrival as well as reflections off targets that are characterized by a delay τ and a Doppler shift f_d . We adopt a narrow-band model here where a signal $x(t)$ of center frequency f_c , will only experience a phase rotation or Doppler shift $f_d = a f_c$; time compression or dilation is assumed negligible and a is the ratio of range-rate to speed of light. Indexing the return of the p th arrival and its associated Doppler shift and delay, the received signal is

$$y(t) = \sum_p A_p e^{j2\pi a_p f_c t} x(t - \tau_p) + w(t), \quad (5)$$

where $w(t)$ is additive noise and A_p is the attenuation including path loss, reflection, and any processing gains. The delays τ_p and Doppler shifts $a_p f_c$ are assumed to be constant during the integration time. In (5) we assume that down-conversion has been performed at the receiver, such that $\tilde{y}(t) = \text{Re} \{ e^{j2\pi f_c t} y(t) \}$. We only refer to the baseband signals in the following.

C. Matched Filter Receiver

The standard approach is to “search” for targets using a bank of correlators tuned to the waveform given a certain Doppler shift and delay, i.e., a matched filter. As an example, the k th correlator will produce for every $\hat{\tau}$ and a fixed Doppler shift $\hat{a}_k f_c$,

$$z_k(\hat{\tau}) = \int_0^{T_i} e^{-j2\pi \hat{a}_k f_c t} x^*(t - \hat{\tau}) y(t) dt. \quad (6)$$

Due to limitations in signal processing complexity, the delay dimension $\hat{\tau}$ is usually only evaluated at discrete points, as

¹This is reasonable due to the application of error correcting codes in digital broadcast signals.

well. As waveforms with varying parameterizations are not orthogonal, for a given target multiple non-zero correlator outputs are generated, which can be described by the ambiguity function [25],

$$U(\hat{\tau}, \hat{a}) = \int_{-\infty}^{\infty} e^{-j2\pi\hat{a}f_c t} x^*(t - \hat{\tau})x(t) dt. \quad (7)$$

The integration time in (6) can be chosen within bounds, limited from below by the necessary integration gain to detect targets and from above by the target coherence time (time variability of A_p) and target motion (τ_p and a_p).

As the transmission $x(t)$ is divided into blocks of length T' , see (3), each consisting of a signal of length T and a cyclic extension of length T_{cp} , assuming that the largest possible delay is smaller than the cyclic extension $\tau_{max} < T_{cp}$, the correlator in (6) can be implemented as²,

$$z_k(\hat{\tau}) = \sum_{i=0}^{T_i/T'} \int_{iT'}^{iT'+T} e^{-j2\pi\hat{a}_k f_c t} x^*(t - \hat{\tau})y(t) dt \quad (8)$$

$$= \sum_{i=0}^{T_i/T'} e^{-j2\pi\hat{a}_k f_c iT'} z_k^{(i)}(\hat{\tau}). \quad (9)$$

The integration time T_i is chosen as an integer multiple of T' , which means we coherently combine a certain number of OFDM blocks, and we define the correlator output of the i th block as,

$$z_k^{(i)}(\hat{\tau}) = \int_0^T e^{-j2\pi\hat{a}_k f_c t} x^*(t + iT' - \hat{\tau})y(t + iT') dt. \quad (10)$$

For OFDM signals the block correlation operation in (10) can be efficiently implemented using the fast Fourier transform (FFT). This is further simplified since due to the cyclic prefix, the correlation operation is actually cyclic in an interval of length T . We write this as,

$$z_k^{(i)}(\hat{\tau}) = \int_0^T x_i^*(t - \hat{\tau}) e^{-j2\pi\hat{a}_k f_c t} y(t + iT') dt \quad (11)$$

$$= \int_0^T \sum_{n=-N/2}^{N/2-1} s_i^*[n] e^{-j2\pi n \Delta f (t - \hat{\tau})} \times e^{-j2\pi\hat{a}_k f_c t} y(t + iT') dt \quad (12)$$

$$= \sum_{n=-N/2}^{N/2-1} \left(e^{j2\pi n \Delta f \hat{\tau}} s_i^*[n] \times \int_0^T e^{-j2\pi n \Delta f t} [e^{-j2\pi\hat{a}_k f_c t} y(t + iT')] dt \right) \quad (13)$$

In words, there are four steps, corresponding to the parentheses, from inside out:

- 1) compensation for the phase rotation in the time domain caused by the Doppler shift;

²We point out that by not using the signal information in the cyclic extension, the SNR is reduced by T/T' , but the processing is greatly simplified by making the output a cyclic convolution with the channel impulse response; this is the standard approach in OFDM receiver processing.

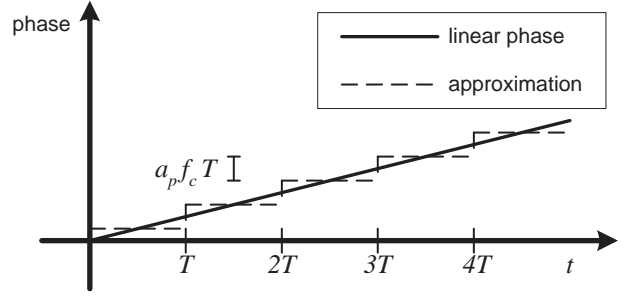


Fig. 3. The phase rotation due to the Doppler shift is approximated as constant over a block duration T' , but since the total integration time encompasses many blocks, the slope can still be estimated through the accumulated phase change using a Fourier transform.

- 2) integration over t - in practice an FFT operation of the sampled signal - giving N outputs for each subcarrier;
- 3) compensation of the (assumed known) data symbols $s_i^*[n]$; and
- 4) inverse FFT operation across various delays.

The output will be correlation values for given delay $\hat{\tau}$ and Doppler $\hat{a}_k f_c$ for the i th OFDM block, the outputs for all blocks have to be combined as given in (9).

III. EFFICIENT MATCHED FILTER BASED ON SIGNAL APPROXIMATION

A. Small Doppler Approximation

Often, the integration time is almost on the order of a second, this means that a very large number of OFDM blocks are included $T' \ll T_i$. When the product between T' and the Doppler shifts is small compared to unity, we can approximate the phase rotation within one OFDM block as constant,

$$e^{-j2\pi\hat{a}_k f_c t} \approx e^{-j2\pi\hat{a}_k f_c (T/2)} \forall t \in [0, T]. \quad (14)$$

Then the Doppler shift has to be estimated based on the increasing accumulated phase shift between consecutive blocks (see Fig. 3), and only a single correlator is needed, as (13) can be simplified to

$$z_k^{(i)}(\hat{\tau}) = \sum_{n=-N/2}^{N/2-1} \left(e^{j2\pi n \Delta f \hat{\tau}} s_i^*[n] \times \int_0^T e^{-j2\pi n \Delta f t} \left[e^{-j\pi\hat{a}_k f_c T} y(t + iT') \right] dt \right) \quad (15)$$

$$= e^{-j\pi\hat{a}_k f_c T} \sum_{n=-N/2}^{N/2-1} e^{j2\pi n \Delta f \hat{\tau}} H_n^{(i)}, \quad (16)$$

where $H_n^{(i)}$ corresponds to the channel estimate of the n th frequency in the i th block ignoring inter-carrier-interference (ICI), and the phase rotation out front is constant and can usually be ignored. With this, the final matched filter output

can be written as,

$$|z_k(\hat{\tau})| = \left| \sum_{i=0}^{T_i/T'} \sum_{n=-N/2}^{N/2-1} e^{-j2\pi(i\hat{a}_k f_c T' - n\Delta f \hat{\tau})} H_n^{(i)} \right|, \quad (17)$$

which is a two-dimensional discrete Fourier transform (DFT) of the OFDM channel estimates that can be efficiently implemented as an FFT.

B. Link to Uniform Rectangular Array

As the operation in (17) is identical to direction finding with a uniform rectangular array (URA), we take a closer look at the channel estimates. Assuming no noise and only a single target present with amplitude A_0 , delay τ_0 and Doppler $a_0 f_c$, we calculate

$$H_n^{(i)} = s^*[n] \int_0^T e^{-j2\pi n \Delta f t} y(t + iT') dt \quad (18)$$

$$= s^*[n] \int_0^T e^{-j2\pi n \Delta f t} \times \left(A_0 x_i(t - \tau_0) e^{j2\pi a_0 f_c (t + iT')} \right) dt \quad (19)$$

$$= A_0 \sum_{m=-N/2}^{N/2-1} s[m] s^*[n] e^{-j2\pi m \Delta f \tau_0} \times \int_0^T e^{-j2\pi(n-m)\Delta f t} e^{j2\pi a_0 f_c (t + iT')} dt \quad (20)$$

Using the approximation in (14), all frequencies are orthogonal, hence

$$H_n^{(i)} \approx A_0 T |s[n]|^2 e^{j2\pi(i a_0 f_c T' - n \Delta f \tau_0)}, \quad (21)$$

and the channel estimates have the same form as the receiver elements of a URA, with equivalent element spacing of T' in Doppler and Δf in delay, the total array aperture size is T_i and $B = N\Delta f$ respectively.

C. Cancellation of Dominant Signal Leakage

Due to the fairly long integration time, corresponding to a large URA, the ambiguity function will be relatively sharp. So interference from other targets will not be an issue except for very close targets. Of concern is the clutter – since the ambiguity function has a “sinc” like shape – the attenuation is relatively slow, leading to significant leakage into the non-zero Doppler bins [7]. As the clutter stems from direct and almost direct arrivals that are easily 50 dB stronger than the targets, the leakage will affect even targets of significantly non-zero Doppler.

One approach is to evaluate the matched filter only at what corresponds to the zeros of the sinc shape, avoiding leakage, but greatly reducing resolution. Another approach is to remove the direct signals using adaptive signal processing on the digital data. This can be done simply by least-squares fitting the received data to a template assuming no time variation (nulling only zero Doppler) or a very limited degree of change (fitting can be easily achieved using a Fourier basis). After the signal components corresponding to these Doppler values

have been approximated, we simply subtract them out of the digitally available signal. This leads to a blind spot of variable size (depending on the least-squares model), but significantly limits the leakage of the dominant signal components.

We will see later that the combination of efficiently implemented matched filter with adaptive signal processing works reasonably well in practice, at low complexity. This will therefore serve as our baseline comparison in regard to other algorithms.

IV. 2D-FFT MUSIC

A. Subspace Construction via Spatial Smoothing

As outlined in Section III-B, we have a signal model that is completely equivalent to the one of N_p wavefronts impinging on a grid of sensors, where the steering vectors have amplitudes A_p .

$$H_n^{(i)} = \sum_{p=1}^{N_p} A_p e^{j2\pi(i\hat{a}_p f_c T' - n\Delta f \hat{\tau}_p)} \quad (22)$$

The azimuth and elevation direction angles are just displaced by delay and Doppler. In order to use subspace methods like “multiple signal classification” (MUSIC), see e.g. [26], several snapshots of the wavefronts are required. We have $i = 1, \dots, L$ ($L = T_i/T'$) OFDM symbols, each consisting of $n = 1, \dots, N$ channel estimates, corresponding to our virtual URA. Since i corresponds to time, the time variations of the multi-path amplitudes A_p could be exploited, to generate independent snapshots at a cost of a smaller equivalent aperture. Typically the alteration in time is not significant enough on the time scale we are considering, therefore we will apply spatial smoothing instead (see e.g. [27] or [26]).

Spatial smoothing can be used to generate the necessary snapshots, where the time variation of the amplitudes is replaced by exploiting shift invariances between the steering vectors corresponding to certain subarrays of the full URA. In a nutshell, when considering two subarrays of a certain shift, they will only vary in a phase shift, but which is different for each signal component, allowing us to construct a full-rank set of observation vectors, again at the cost of a smaller equivalent aperture.

To define a steering vector, we denote the response of one array element to a wave of $(\hat{\tau}, \hat{a})$ as

$$b_{n,i}(\hat{\tau}, \hat{a}) = e^{j2\pi(i\hat{a} f_c T' - n\Delta f \hat{\tau})} \quad (23)$$

and define a subarray matrix, indexed by n' and i' , of reduced dimension $N' \times L'$:

$$\mathbf{B}_{n',i'}(\hat{\tau}, \hat{a}) = \begin{bmatrix} b_{n',i'} & \dots & b_{n',i'+L'-1} \\ \vdots & & \vdots \\ b_{n'+N'-1,i'} & \dots & b_{n'+N'-1,i'+L'-1} \end{bmatrix}. \quad (24)$$

The total number of subarrays we generate this way, must be larger than the number of multipath components, and is given by

$$N_{\text{sub}} = (N - N' + 1)(L - L' + 1) > N_p. \quad (25)$$

Next, we use the $\text{vec}\{\cdot\}$ -operation, which takes a matrix column-wise in order to construct a vector from it, and define a steering vector

$$\mathbf{b}_{n',i'}(\hat{\tau}, \hat{a}) = \text{vec}\{\mathbf{B}_{n',i'}(\hat{\tau}, \hat{a})\}. \quad (26)$$

We have the shift invariances

$$\mathbf{b}_{n'+1,i'}(\hat{\tau}_p, \hat{a}_p) = e^{-j2\pi\Delta f\hat{\tau}_p} \mathbf{b}_{n',i'}(\hat{\tau}_p, \hat{a}_p) \quad (27)$$

$$\mathbf{b}_{n',i'+1}(\hat{\tau}_p, \hat{a}_p) = e^{j2\pi\hat{a}_p f_c T'} \mathbf{b}_{n',i'}(\hat{\tau}_p, \hat{a}_p), \quad (28)$$

and, consequently, all vectors $\mathbf{b}_{n',i'}(\hat{\tau}_p, \hat{a}_p)$ are linearly dependent.

In the same way, we can group the channel estimates $H_n^{(i)}$ in subarrays and stack the columns of each matrix on top of each other. We can write the signal model for these vectors as

$$\mathbf{h}_{n',i'} = \sum_{p=1}^{N_p} A_p \mathbf{b}_{n',i'}(\hat{\tau}_p, \hat{a}_p). \quad (29)$$

Due to the above shift-invariances we find

$$\mathbf{h}_{n'+m,i'+l} = \sum_{p=1}^{N_p} A_p e^{j2\pi(l\hat{a}_p f_c T' - m\Delta f\hat{\tau}_p)} \mathbf{b}_{n',i'}(\hat{\tau}_p, \hat{a}_p), \quad (30)$$

i.e. we have a new 'snapshot', where the signals

$$\hat{A}_p = A_p e^{j2\pi(l\hat{a}_p f_c T' - m\Delta f\hat{\tau}_p)} \quad (31)$$

passed the same subarray.

From these snapshots we can build an $(N' \cdot L') \times N_{\text{sub}}$ observation matrix,

$$\mathbf{A} = [\mathbf{h}_{1,1} \ \cdots \ \mathbf{h}_{N-N'+1,1} \ \cdots \ \mathbf{h}_{N-N'+1,L-L'+1}]. \quad (32)$$

The signal and noise subspace, $\mathbf{U}^{(s)}$ and $\mathbf{U}^{(n)}$, can be obtained via a SVD,

$$\mathbf{A} = \mathbf{U}\mathbf{D}\mathbf{V}, \quad (33)$$

with \mathbf{U} and \mathbf{V} being size $(N' \cdot L')$ and N_{sub} unitary matrices respectively, and $\mathbf{U} = [\mathbf{U}^{(s)} \ \mathbf{U}^{(n)}]$ is split such that the vectors in $\mathbf{U}^{(s)}$ correspond to the N_p largest singular values. The MUSIC cost-function can be given either in terms of the noise subspace or signal subspace respectively,

$$f_{\text{MUSIC}}(\hat{\tau}, \hat{a}) = \left(\left| \mathbf{b}^H(\hat{\tau}, \hat{a}) \mathbf{U}^{(n)} \right|^2 \right)^{-1} \quad (34)$$

$$= \left(N' L' - \left| \mathbf{b}^H(\hat{\tau}, \hat{a}) \mathbf{U}^{(s)} \right|^2 \right)^{-1}, \quad (35)$$

where we have dropped the indices of the subarray steering vector \mathbf{b} , as due to the shift invariance any one of the subarrays could be chosen.

B. Efficient Implementation as FFT

As a first step, there is an advantage of expressing the MUSIC cost function in terms of the signal subspace, due to the fact that the dimension $N' L' \approx 10^5$, whereas the number of signal eigenvectors N_p is only on the order of a few hundred, i.e., under these conditions it is much "cheaper" to work with the signal subspace which is obtained via a "short" SVD of the subarrays.

We further change the evaluation of the MUSIC cost-function to use the FFT. Let the N_p -dimensional signal subspace be partitioned into

$$\mathbf{U}^{(s)} = [\mathbf{u}_1 \ \cdots \ \mathbf{u}_{N_p}], \quad (36)$$

then we have

$$f_{\text{MUSIC}}(\hat{\tau}, \hat{a}) = \left(N' L' - \sum_{p=1}^{N_p} \left| \mathbf{b}^H(\hat{\tau}, \hat{a}) \mathbf{u}_p \right|^2 \right)^{-1}. \quad (37)$$

As in the case of the matched filter, we will not practically be able to evaluate the cost-function for any combination of $\hat{\tau}$ and \hat{a} , but instead consider possible discrete values, commonly arranged in a grid fashion. We next consider the individual terms in the sum in (37) and show that when evaluating them for $\hat{\tau}$ and \hat{a} values on a grid, the computation can be put into the format of a two-dimensional Fast Fourier Transform that allows efficient evaluation.

In the following we make use of a formula involving the Kronecker product and the vec -operation, which was derived by Magnus and Neudecker [28]:

$$\text{vec}\{\mathbf{ABC}\} = (\mathbf{C}^T \otimes \mathbf{A}) \text{vec}\{\mathbf{B}\}. \quad (38)$$

Defining the matrix \mathbf{U}_p by $\mathbf{u}_p = \text{vec}\{\mathbf{U}_p\}$ and using the fact that the steering vector of the rectangular array can be written as the Kronecker product of two steering vectors with elements,

$$\mathbf{b}^{(N')}(\hat{\tau}) = [e^{-j2\pi\Delta f\hat{\tau}} \ \cdots \ e^{-j2\pi N' \Delta f\hat{\tau}}]^T \quad (39)$$

$$\mathbf{b}^{(L')}(\hat{a}) = [e^{j2\pi\hat{a} f_c T'} \ \cdots \ e^{j2\pi L' \hat{a} f_c T'}]^T, \quad (40)$$

we find that

$$\mathbf{b}^H(\hat{\tau}, \hat{a}) \mathbf{u}_p = (\mathbf{b}^{(L')}(\hat{a}) \otimes \mathbf{b}^{(N')}(\hat{\tau}))^H \mathbf{u}_p \quad (41)$$

$$= (\mathbf{b}^{(L')}(\hat{a}) \otimes \mathbf{b}^{(N')}(\hat{\tau}))^H \text{vec}\{U_p\} \quad (42)$$

$$= (\mathbf{b}^{(L')H}(\hat{a}) \otimes \mathbf{b}^{(N')H}(\hat{\tau})) \text{vec}\{U_p\} \quad (43)$$

$$= \text{vec}\{\mathbf{b}^{(N')H}(\hat{\tau}) U_p \mathbf{b}^{(L')*}(\hat{a})\} \quad (44)$$

$$= \mathbf{b}^{(N')H}(\hat{\tau}) U_p \mathbf{b}^{(L')*}(\hat{a}). \quad (45)$$

When inspecting the definition of $\mathbf{b}^{(N')}(\hat{\tau})$ and $\mathbf{b}^{(L')}(\hat{a})$, we see that they are columns of a DFT matrix if we define

$$\hat{\tau} = 0, T/N', \dots, (N' - 1)T/N', \quad (46)$$

$$\hat{a} = 0, 1/(f_c T' L'), \dots, (L' - 1)/(f_c T' L'). \quad (47)$$

Accordingly, the MUSIC cost-function can be evaluated using N_p two-dimensional FFTs, which are summed up in magnitude. The FFTs can be performed with additional zero-padding to evaluate a denser grid of tentative values of $\hat{\tau}$ and \hat{a} .

C. Pseudo-Code of the MUSIC Implementation

Define:

$$\mathbf{h}_m = \text{vec}(\mathbf{H}_m)$$

- 1) Remove the direct-blast with Doppler high-pass filtering

- 2) Project on the space orthogonal to the stationary components: Perform an eigen-decomposition of the matrix of all channel estimates

$$\begin{aligned}\mathbf{R} &= [\mathbf{h}_1, \dots, \mathbf{h}_M] \\ \mathbf{R}^H \mathbf{R} &= \mathbf{U} \mathbf{\Sigma} \mathbf{U}^H \\ \mathbf{U}_r &= \mathbf{R} \mathbf{U}(:, 1 : M_r) \mathbf{\Sigma}^{-1/2} \\ \mathbf{h}_m &= (\mathbf{I} - \mathbf{U}_r \mathbf{U}_r^H) \mathbf{h}_m\end{aligned}$$

- 3) 2D-FFT-MUSIC

$$\mathbf{X}_m = \text{reshape}(\hat{\mathbf{h}}_m, N, L)$$

Select K shifted sub-arrays $\mathbf{X}_s^{(k)}$ and 'vectorize' them

$$\mathbf{x}^{(k)} = \text{vec}(\mathbf{X}_s^{(k)})$$

Perform an eigen-decomposition of the matrix of all sub-array-vectors

$$\begin{aligned}\mathbf{R}_s &= [\mathbf{x}^{(1)}, \dots, \mathbf{x}^{(K)}] \\ \mathbf{R}_s^H \mathbf{R}_s &= \mathbf{U}_s \mathbf{\Sigma}_s \mathbf{U}_s^H \\ \mathbf{B}_s &= \mathbf{U}_s(:, 1 : N_{ev}) \cdot \mathbf{\Sigma}_s^{-1/2} \\ \mathbf{F} &= \sum_{n=1}^{N_{ev}} \text{FFT2}(\text{reshape}(\mathbf{R}_s \cdot \mathbf{B}_s(:, n), N', L'))^2\end{aligned}$$

V. COMPRESSED SENSING

A. Non-linear Estimation via Sparse Estimation

Similar to the subspace approach, we use the OFDM channel estimates as measurements. This has no loss in information, as the bandlimited signal can be exactly represented by a sufficient number of frequency estimates. Using the same simplifications from (21) and the definition of steering vectors in (24) and (26), we write the measurement model as in (29),

$$\mathbf{h} = \sum_{p=1}^{N_p} A_p \mathbf{b}(\hat{\tau}_p, \hat{a}_p) + \mathbf{w}, \quad (48)$$

but where we drop the indices connected to subarrays and include noise explicitly. We can reasonably assume that the noise is still circular-symmetric complex Gaussian of Power N_0 (the information symbols $s_i[n]$ are unit amplitude). Defining the following notation,

$$\mathbf{B}_{N_p} = [\mathbf{b}(\hat{\tau}_1, \hat{a}_1) \quad \dots \quad \mathbf{b}(\hat{\tau}_{N_p}, \hat{a}_{N_p})] \quad (49)$$

$$\mathbf{a}_{N_p} = [A_1 \quad \dots \quad A_{N_p}]^T \quad (50)$$

we can rewrite the model as

$$\mathbf{h} = \mathbf{B}_{N_p} \mathbf{a}_{N_p} + \mathbf{w}. \quad (51)$$

We see that if we knew the N_p pairs of $(\hat{\tau}_p, \hat{a}_p)$, we could construct \mathbf{B}_{N_p} and solve for \mathbf{a}_{N_p} via a simple least-squares solution.

$$\hat{\mathbf{a}}_{N_p} = \arg \min_{\mathbf{a}_{N_p}} \|\mathbf{h} - \mathbf{B}_{N_p} \mathbf{a}_{N_p}\|^2 \quad (52)$$

Of course if we had a set of $(\hat{\tau}_p, \hat{a}_p)$ we already knew where the targets were and wouldn't need the amplitude values A_p ,

but estimating the amplitudes lets us confirm targets, e.g., if we had a larger list of possible targets constituting a larger matrix \mathbf{B} . This is essentially what the matched filter does, we look at the "energy" at potential target locations, whereby the least-squares solution is replaced by the correlation operation as in,

$$\hat{\mathbf{a}}_{\text{MF}} = \mathbf{B}^H \mathbf{h}, \quad (53)$$

since we generally have more tentative target tuples $(\hat{\tau}_p, \hat{a}_p)$ as measurements, making the matrix \mathbf{B} "fat". One special case is when we choose just as many tentative tuples $(\hat{\tau}_p, \hat{a}_p)$ as there are observations on an evenly spaced grid. As pointed out in the previous section on MUSIC, the columns of \mathbf{B} are then the coefficients of a two-dimensional Fourier transform and therefore orthogonal, making the least-squares and correlation solutions equal.

A different approach to solve (52) without explicit knowledge of the $(\hat{\tau}_p, \hat{a}_p)$ is using sparse estimation. In a nutshell, we solve the least-squares problem by additionally enforcing that the solution should be based on the assumption that there are only few targets, i.e., the solution $\hat{\mathbf{a}}_{\text{CS}}$ should be sparse (few non-zero entries).

B. Orthogonal Matching Pursuit

In our earlier work [13], we employed a low complexity algorithm, Orthogonal Matching Pursuit (OMP) [19], [20]. This greedy algorithm uses the matched filter outputs to detect the strongest target and associated $(\hat{\tau}_p, \hat{a}_p)$, solves (52) and subtracts the influence of this target from all correlator outputs, similar to serial interference cancellation. This is repeated until "enough" targets have been identified, usually determined based on all adjusted correlator outputs being lower than a threshold.

Although good results on simulation data were achieved, [13], OMP proved to have problems on experimental data. This seems to have been due to two reasons: i) there are a large amount of clutter and direct signals, leading to high complexity since the algorithm's run time scales with the number of targets (clutter count as stationary targets); ii) more importantly, there is always some modeling inaccuracy, e.g., due to only considering a grid of possible $(\hat{\tau}_p, \hat{a}_p)$. The modeling inaccuracy is usually a minor concern, but since the direct arrivals are more than 50 dB stronger than the targets, when the correlator outputs are adjusted, these inaccuracies lead to residuals on the same order or larger than the targets. Furthermore these residuals do not decrease in value quickly with each iteration of the algorithm as they do not match the vectors in \mathbf{B} well. Removing the clutter as in the conventional FFT based processing did not lead to significant improvement either, which lead us to employ Basis Pursuit instead.

C. Basis Pursuit

Instead of trying to construct the matrix \mathbf{B}_{N_p} by identifying targets iteratively, Basis Pursuit (BP) uses the so-called l_1 -norm regularization term [21]–[23],

$$\|\mathbf{x}\|_1 = \sum_i |x_i|. \quad (54)$$

carrier frequency	f_c	227.36 MHz
subcarrier spacing	Δf	1 kHz
no. subcarriers	N	1537
bandwidth	B	1.537 MHz
symbols length	T	1 ms
cyclic prefix	T_{cp}	0.246 ms
block length	T'	1.246 ms
blocks per frame	L	76
Null symbol	T_{NULL}	1.297 ms
frame duration	T_F	96 ms

TABLE I
OFDM SIGNAL SPECIFICATIONS OF DAB ACCORDING TO ETSI 300 401 [24].

With this the problem is formulated as,

$$\text{minimize } |\mathbf{h} - \mathbf{B}\mathbf{a}|^2 + \lambda|\mathbf{a}|_1, \quad (55)$$

where λ determines the ‘‘sparsity’’ of the solution and \mathbf{a} can have significantly higher dimension than \mathbf{h} without detrimental effect on the solution.

The problem formulation in (55) is a convex optimization problem. Various efficient implementations have been suggested in the literature [29], [30]. Since baseband data is generally complex valued, the definition in (54) becomes,

$$|\mathbf{x}|_1 = \sum_i \sqrt{|\text{Re}\{x_i\}|^2 + |\text{Im}\{x_i\}|^2}. \quad (56)$$

We implemented the algorithm outlined in the appendix of [29] as an extension to the real case. It is based on an interior point method using approximate Newton search directions.

Both the OMP and BP can be implemented more efficiently by noticing that the multiplication with \mathbf{B} can be implemented using FFT operations as long as the $\hat{\tau}$ and \hat{a} are chosen on an evenly spaced grid (see Sect. IV-B). This leads to an almost linear complexity in the number of observations ($N \cdot L$) and number of tentative target parameters ($\hat{\tau}_p, \hat{a}_p$), whereby due to zero-padding in the FFT operation the larger number dominates (number of tentative target parameters).

VI. NUMERICAL SIMULATION

A. Simulation Setup

The signal is simulated as,

$$y(t) = \sum_p A_p x(t - \tau_p(t)) + w(t) \quad (57)$$

where $\tau_p(t)$ is the exact bi-static delay. The definition of bi-static delay for a signal transmitted from \mathbf{x}_s , received at \mathbf{x}_r , and reflected off a target at $\mathbf{x}(t)$ is:

$$\tau(t) = \frac{1}{c} (|\mathbf{x}(t) - \mathbf{x}_r| + |\mathbf{x}_s - \mathbf{x}(t)| - |\mathbf{x}_r - \mathbf{x}_s|). \quad (58)$$

For simulation purposes we generate receiver data at a sampling rate of 2.048 MHz, the bi-static delays are updated at the same rate. The target is simulated as a point target, but the auto-correlation of $A_p(t)$ over time is modeled based on a five-point extended target assumption, similar as in [18]. The target size is assumed at a diameter of about 30 m (only for the auto-correlation of $A_p(t)$). The RCS with respect to different

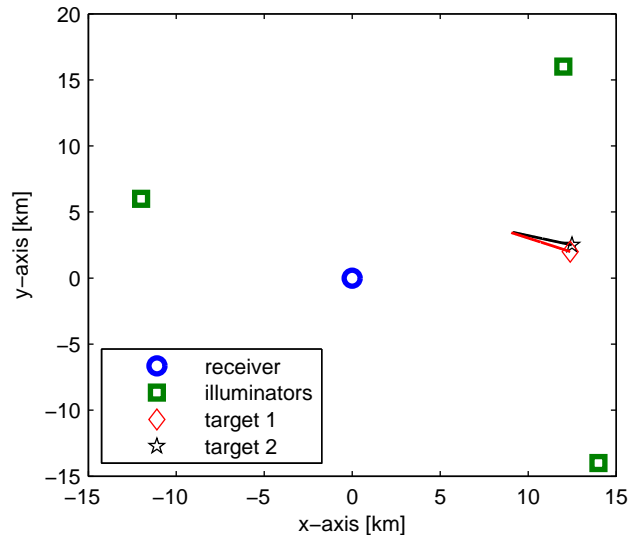


Fig. 4. Simulation setup of one receiver and three DAB stations illuminating two closing targets; the markers are at the target starting positions.

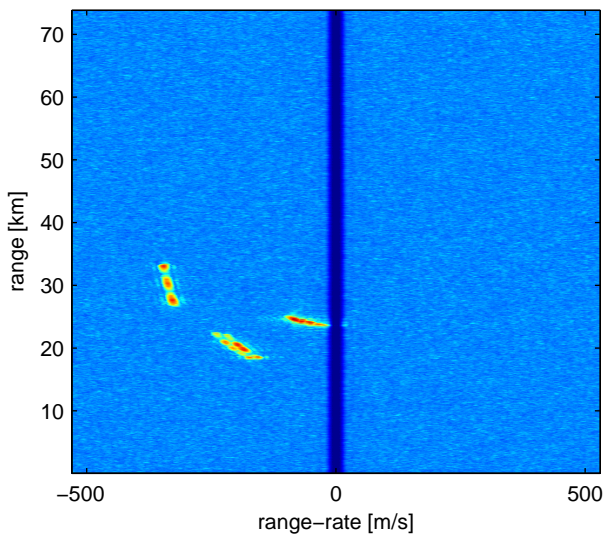
transmitters is assumed to be independent, as these are several kilometers apart.

The DAB signal is specified in [24], for convenience we reproduce most parameters in Tab. I, notation matching ours in Section II. We see that due to the bandwidth of $B = 1.537$ MHz, the spatial resolution is approximately $c/B \approx 195$ m (the speed of light is $c = 3 \times 10^8$ m/s). Therefore for assumed targets of 30 m diameter, the point target model seems reasonable. This could be quite different when using a DVB signal of larger bandwidth.

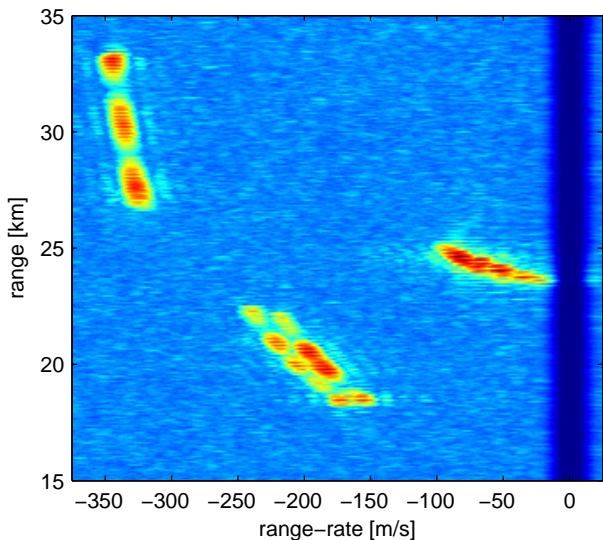
One of the main assumptions to test in the simulation is the small Doppler approximation. Accordingly we simulate targets at a relatively high speed that will lead to significant Doppler shifts. The scenario is shown in Fig. 4, where three radio towers illuminate two targets, the receiver is placed at the origin. The targets are moving at constant velocity of about 180 m/s, approaching each other slowly with simulation time, c.f. Fig. 4. We simulate 200 DAB frames, for a total time of 18.2 s, in which the targets cover about 3.5 km.

The SNR of the direct signal is about 20 dB, at which any regular DAB receiver would operate virtually error free, this makes our assumption of perfect signal reconstruction well justified. We fix each target at -30 dB (per sample), leading to a difference of 50 dB between direct arrival and target signatures. We do not specifically consider any transmitter or receiver gain, attenuation based on distance traveled or signal frequency, as we directly generate digital samples at the output. Knowing that the targets follow a Swerling I model (due to the extended target model), we will need about 20 dB SNR to detect the targets reliably. We therefore coherently combine one OFDM frame, which leads to an integration gain of $T_F \cdot B \approx 50$ dB, but doesn't affect the ratio between targets and direct blast (see [7] for a detailed discussion of integration gain calculation).

To see the performance of the super-resolution methods, we use two targets which move on trajectories bringing them



(a) Conventional FFT Processing



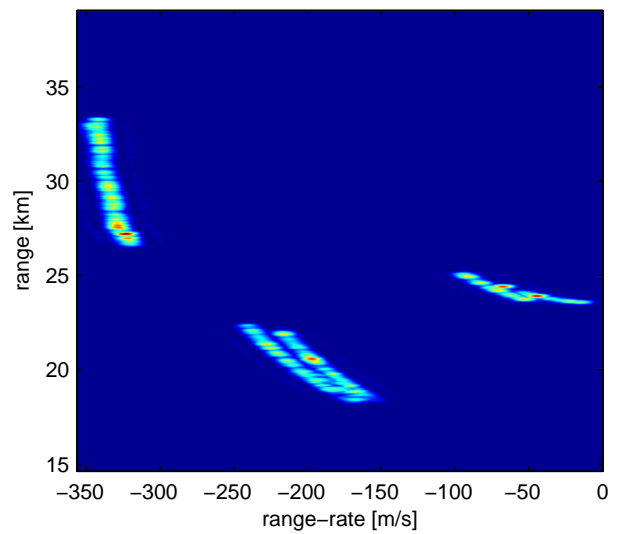
(b) Zoom

Fig. 5. Simulation results using conventional FFT processing, due to three illuminators and two targets we should discern six signatures; (a) in the full view we see the gap left by the direct signal subtraction, the target speeds of about 180 m/s lead to range-rates up to double that amount; (b) in the zoomed view we notice that although the targets are easily detected at this SNR, the target separation is weak using the matched filter.

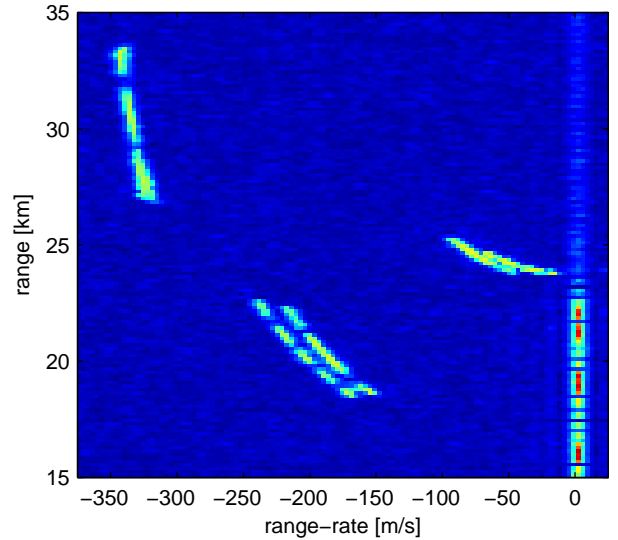
closer during simulation time. This will let us evaluate the target resolution.

B. Simulation Results

We first take a look at the results using conventional FFT processing, see Fig. 5, the figure shows the superposition of the algorithm outputs over all frames. After subtracting the direct signal, the results look fairly “clean”. Some speckle indicates the noise floor, making the subtracted region show up clearly. We notice that even the target signatures appearing at high range-rate are easily detected: a range-rate of $\dot{r} = 400$ m/s corresponds to a phase rotation of about $\dot{r}/c \cdot f_c T \cdot 2\pi \approx 0.6\pi$. In further simulation studies we found that even for close to a



(a) MUSIC



(b) Basis Pursuit

Fig. 6. Both MUSIC and compressed sensing remove the sidelobes of the targets; resolving the targets better than the conventional FFT processing baseline comparison; while MUSIC still needs to subtract the direct signal first, compressed sensing is not affected by the much stronger direct signal (50 dB).

half phase rotation during one OFDM symbol, the target loses only about 3 dB.

In the zoomed view of Fig. 5(b), we also notice that the signal amplitude fades due to our extended target model. Using conventional FFT processing the targets are not resolved, due to the large sidelobes. On the contrary, the super-resolution methods both fully remove the sidelobes, see Fig. 6. While MUSIC needs to use the same direct signal subtraction as the conventional FFT processing, our compressed sensing implementation via Basis Pursuit can handle the direct blast within its framework.

The run times are as follows (all on a regular desktop PC using MATLAB), the beamforming algorithm needs about 0.2 s per frame of data, the MUSIC approach is in the tens of seconds, while Basis Pursuit is in the hundreds of seconds.



Fig. 7. Photo of the antenna used to record the experimental data.

Another comment on the compressed sensing algorithms is that OMP runs on the same order as MUSIC (higher tens of seconds) for this simulation data, with identical results, but did not work at all on the experimental data.

VII. EXPERIMENTAL DATA

A. Experimental Equipment

The experimental data was acquired during a measurement campaign conducted by the German Research Establishment for Applied Science (FGAN). The Research Institute for High Frequency Physics and Radar Techniques (FHR) build CORA (Covert Radar), a passive radar receiver, for the purpose of technology demonstration [10]. In CORA, a circular antenna array with elements for the VHF- (150-350 MHz) and the UHF-range (400-700 MHz) is used to exploit alternatively DAB or DVB signals for target illumination. A fiber optic link connects the elevated antenna and RF-front-end with the processing back-end, consisting of a cluster of high power 64-bit processors. Thus, CORA is also a demonstration of the so called “software-defined-radar” principle. Fig. 7 shows the antenna and front-end of the CORA system during installation at the military electronic warfare exercise ELITE 2006.

A circular array antenna with 16 element panels has been realized to avoid mechanically rotating parts. The reflector planes of the panels approximate a cylinder. Each panel holds two element planes. In the current configuration, the lower plane is equipped with crossed butterfly dipoles for horizontal and vertical polarization, which cover the 150 to 350 MHz frequency range and are thus suited for DAB reception. The 16 elements, feeding the 16 receiver channels of the front-end, allow 360° beam forming.

The upper plane is equipped with 16 vertically polarized UHF-broad band dipoles for DVB. Due to the higher frequencies, each panel holds two of these dipoles, horizontally spaced, to allow for beam forming within a field of 0° to 180°. The back half of the upper plane is equipped with spare dipole elements. Alternatively, both planes can be equipped with crossed butterfly dipoles, which can be combined to sharpen

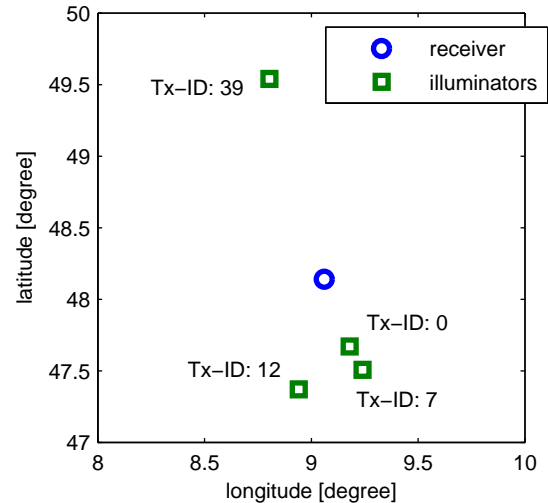


Fig. 8. Overview of DAB stations and receiver in ELITE 2006 experiment.

	lat.	long.	alt.	baseline
Rx	48.14°	9.06°	9,200 m	N/A
Tx 0	47.67°	9.18°	471 m	52.9 km
Tx 7	47.51°	9.24°	564 m	71.7 km
Tx 12	47.37°	8.94°	1164 m	86.0 km
Tx 39	49.54°	8.80°	737 m	157 km

TABLE II
MEASUREMENT SETUP OF ELITE 2006 EXPERIMENT

the beam in elevation. The individual dipole elements in front of the reflector plane each have a cardioid element diagram, providing for approximately 3 dB gain. All elements which are not used in the measurement configuration are terminated with 50 ohms resistors mounted inside the central tower of the array.

The HF-front-end consists of 16 equal receiver channels. Each of the receiver channels comprises of a low-noise amplifier (LNA), a tunable or fixed filter and an adaptive gain control for optimum control of the Analog to Digital Converter (ADC). The LNAs have a noise figure of 1.1 dB and a gain of 40 dB. In the current configuration fixed DAB band-pass filters are being used with a pass band of 220 to 234 MHz. A chirp signal with a bandwidth of 1.536 MHz, centered around 227.36 MHz (226.592-228.128 MHz, channel 12C), generated by a separate signal generator and transmitted to the front-end by coaxial cable, is used for calibration. A bank of switches provides for calibration of each receiver channel chain from the LNA to the ADC, excluding only the antenna element.

The experimental data available was recorded during a measurement campaign in the southern part of Germany, the precise locations can be seen in Table II. There were four active DAB transmitters in the area, the geometry of the setup is depicted in Fig. 8, where we see that one station is to the north (close to Mannheim, Germany), and three more towards the south (around the Swiss border). About six hundred DAB frames, or roughly one minute of recorded data is available. Currently no ground truth in form of radar or air traffic control data is available at this point.

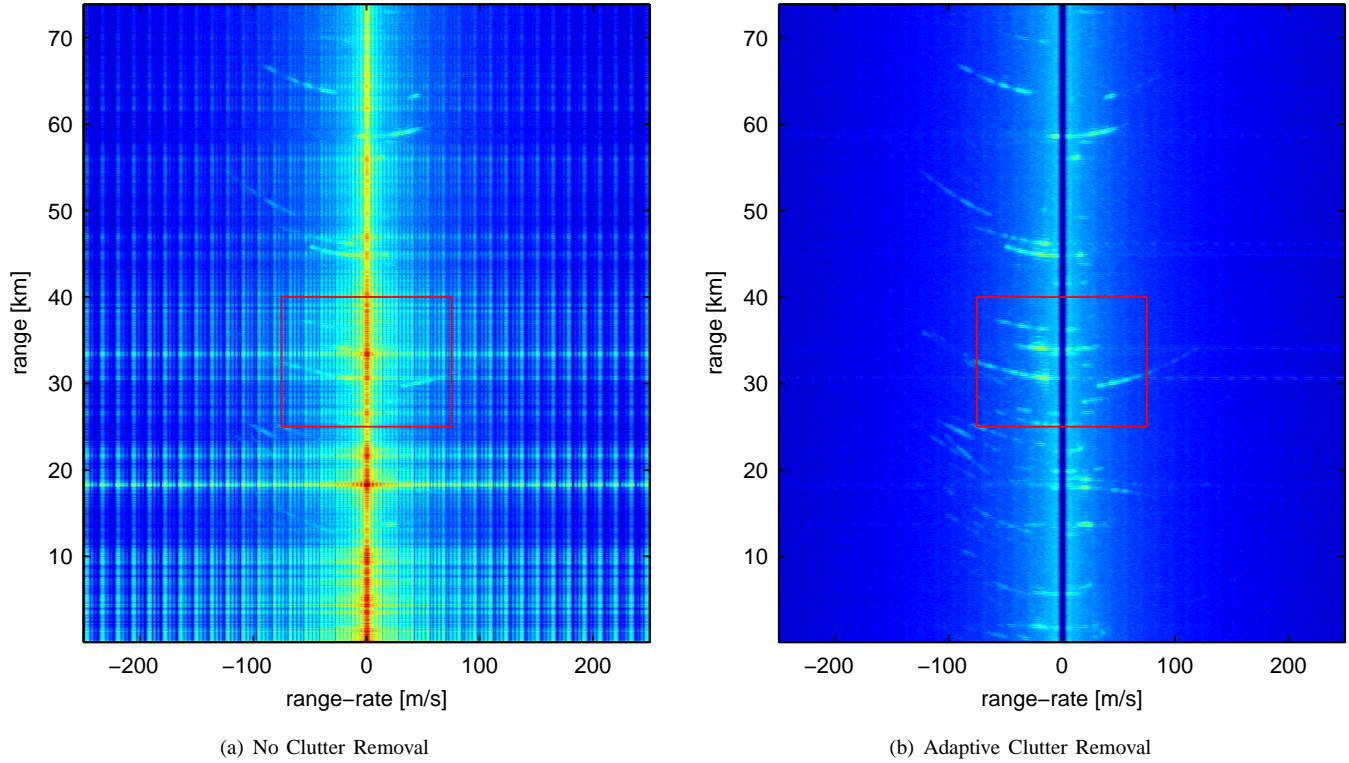


Fig. 9. (a) The conventional FFT based processing suffers heavily from the direct signal leakage; (b) with adaptive clutter removal numerous tracks can be observed.

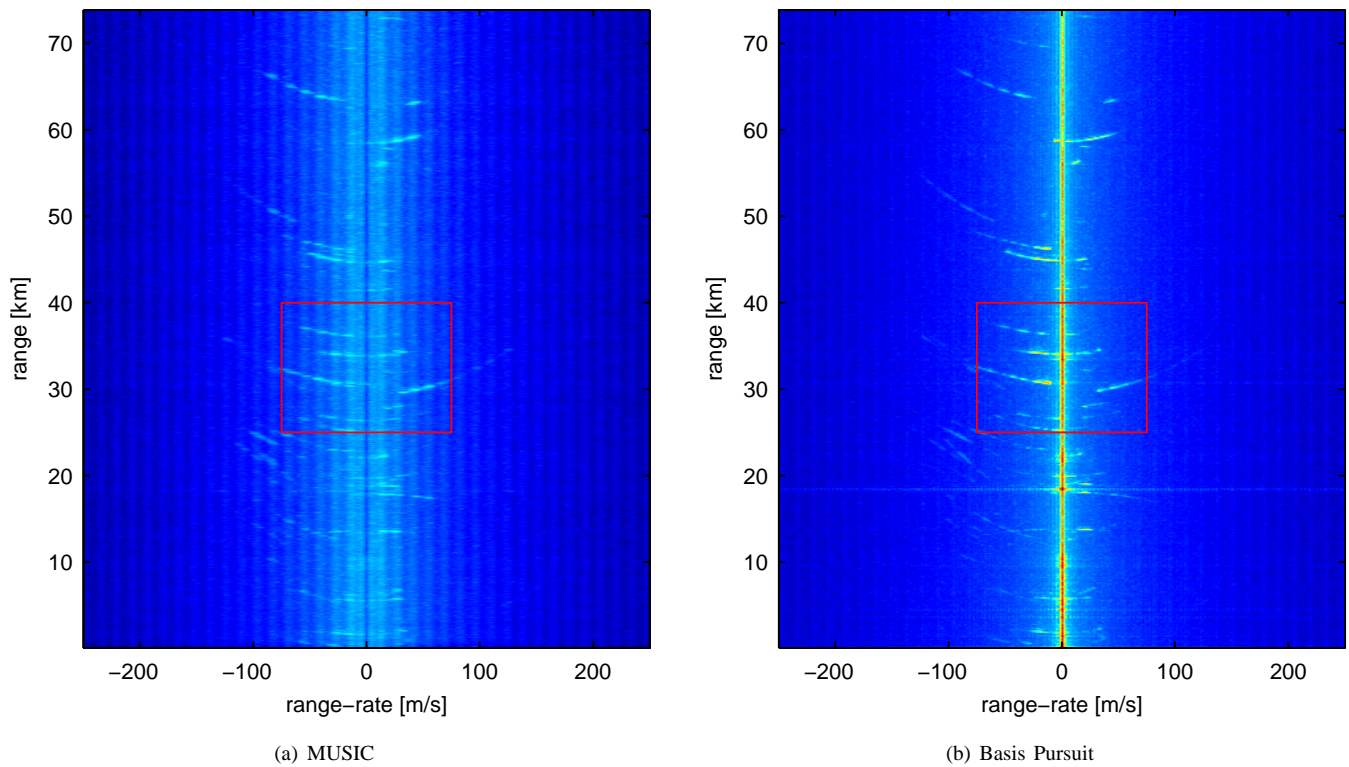


Fig. 10. The high resolution methods work well; while (a) MUSIC needs a similar adaptive clutter removal as the conventional FFT processing, (b) Basis Pursuit can handle the clutter directly.

B. Algorithm Performance

The DAB specifications and algorithm settings are identical as in the simulation study, as it was designed to mirror this scenario. The major difference is that received SNR is lower, due to the quite far observation range. We try to compensate the low SNR by increasing the integration time, instead of combining one DAB frame, we will consider two or four frames (about 200-400 ms).

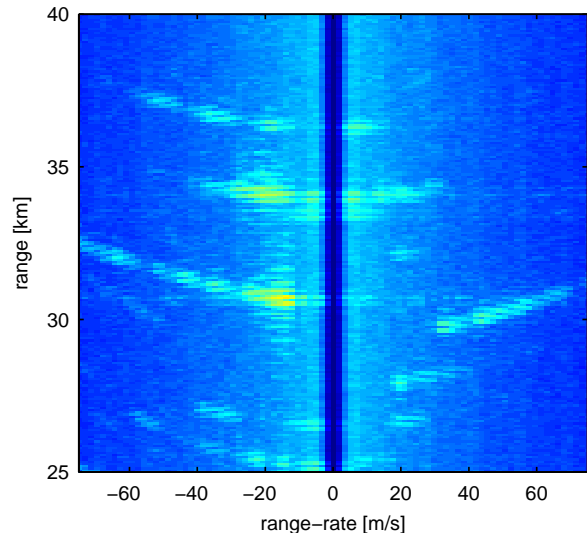
We first examine the results using the conventional FFT processing, see Fig. 9, where we again plot the superposition over all processed frames. To show the effect of leakage due to severe clutter, we also include a plot without the adaptive clutter removal, see Fig. 9(a). After adaptive clutter removal, a number of tracks can be observed. The axis in Fig. 9 and all following figures are limited to 250 m/s, as all target detections occur at lower range-rates.

In the case of MUSIC, the direct signal and clutter removal can also be handled in beamspace. Since the stationary signal components do not change across frames, we simply take a large number of frames and choose the two-hundred largest eigen-vectors. This also benefits from the fact that the targets change across frames, diminishing their effect compared to the stationary signal parts. Each frame is then projected onto this space to remove direct signal and other clutter. In Fig. 10(a), we see that this different approach gives as a softer “gap” around the zero range-rate region compared to Fig. 9. Unfortunately a different type of artifact surfaces as vertical lines. Using compressed sensing in form of Basis Pursuit, the experimental data was processed, see Fig. 10(b).

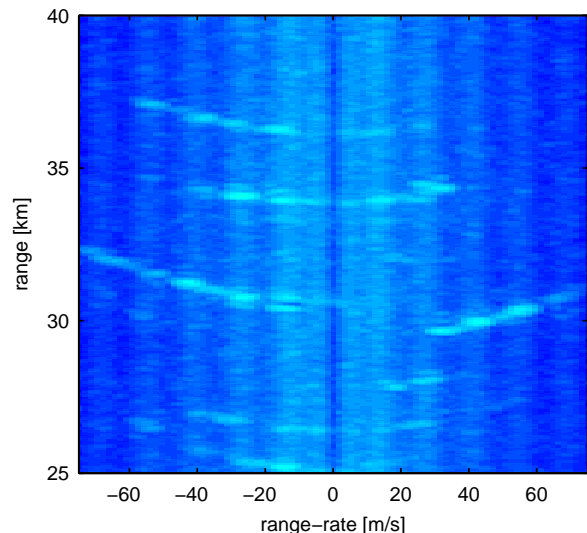
To point out the advantages of the super-resolution methods, we enlarge a central area with several tracks, see Fig. 11. Comparing the results for conventional FFT processing, Fig. 11(a), to MUSIC and Basis Pursuit, see Fig. 11(b) and (c), we can clearly see that the super-resolution methods do not suffer from the same sidelobes like the conventional FFT processing. In addition, Basis Pursuit can detect targets with significantly smaller Doppler values, due to not utilizing any clutter removal.

VIII. CONCLUSION

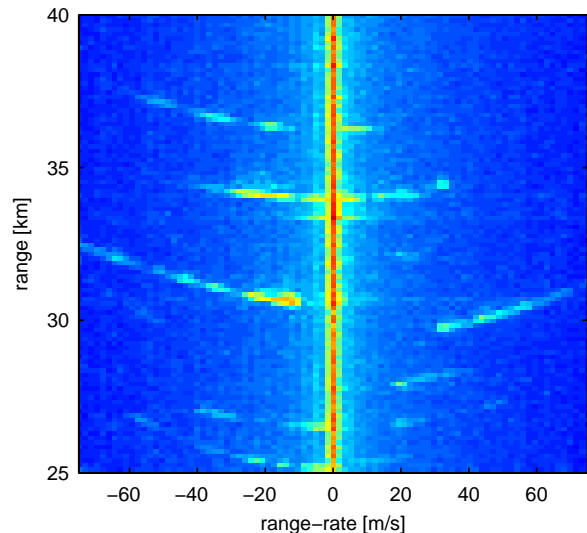
In this paper, we illustrated the passive radar concept and described the current state-of-the-art. We derived the exact matched filter receiver, which was not available before. We showed that a current efficient FFT based approach is equivalent to matched filtering based on a piece-wise constant approximation of the Doppler induced phase rotation on the received waveforms. Using the same approximation we developed efficient implementations of receiver algorithms using subspace concepts, namely MUSIC, and compressed sensing implemented as Basis Pursuit. We discussed the implementation and various benefits of these algorithms, and tested them using numerical simulation and experimental data. We find that in complexity the subspace approach is one order of magnitude higher than the current approach, followed by the Basis Pursuit formulation that is again one order of magnitude more costly in complexity. Nevertheless, high-complexity algorithms achieved higher target resolution



(a) Conventional FFT Processing



(b) MUSIC



(c) Basis Pursuit

Fig. 11. We show an enlarged view to focus on the sidelobe suppression of the high resolution methods.

by avoiding common sidelobes found in conventional FFT based processing. Additionally Basis Pursuit does not require adaptive removal of clutter and the direct signal, leading to better detectability of small Doppler targets.

REFERENCES

- [1] M. Cherniakov, Ed., *Bistatic Radars: Emerging Technology*. John Wiley and Sons, 2008, ch. Passive Bistatic Radar Systems, pp. 247–309.
- [2] H. Kuschel, “VHF/UHF radar part 1: Characteristics,” *Electronics & Communication Engineering Journal*, vol. 14, no. 2, pp. 61–72, Apr. 2002.
- [3] —, “VHF/UHF radar part 2: Operational aspects and applications,” *Electronics & Communication Engineering Journal*, vol. 14, no. 2, pp. 101–111, Apr. 2002.
- [4] P. Howland, “Target tracking using television-based bistatic radar,” *IEE Proc. Radar, Sonar & Navig.*, vol. 146, no. 3, pp. 166–174, Jun. 1999.
- [5] —, “Editorial: Passive radar systems,” *IEE Proc. Radar, Sonar & Navig.*, vol. 152, no. 3, pp. 105–106, Jun. 2005.
- [6] P. Howland, D. Maksimiuk, and G. Reitsma, “FM radio based bistatic radar,” *IEE Proc. Radar, Sonar & Navig.*, vol. 152, no. 3, pp. 107–115, Jun. 2005.
- [7] H. D. Griffiths and C. J. Baker, “Passive coherent location radar systems. Part 1: Performance prediction,” *IEE Proc. Radar, Sonar & Navig.*, vol. 152, no. 3, pp. 153–159, Jun. 2005.
- [8] C. J. Baker, H. D. Griffiths, and I. Papoutsis, “Passive coherent location radar systems. Part 2: Waveform properties,” *IEE Proc. Radar, Sonar & Navig.*, vol. 152, no. 3, pp. 160–168, Jun. 2005.
- [9] D. Poullin, “Passive detection using digital broadcasters (DAB, DVB) with COFDM modulation,” *IEE Proc. Radar, Sonar & Navig.*, vol. 152, no. 3, pp. 143–152, Jun. 2005.
- [10] M. Glende, J. Heckenbach, H. Kuschel, S. Mueller, J. Schell, and C. Schumacher, “Experimental passive radar systems using digital illuminators (DAB/DVB-T),” in *Proc. of Intl. Radar Symposium*, Cologne, Germany, Sep. 2007, pp. 411–417.
- [11] H. Kuschel, J. Heckenbach, S. Mueller, and R. Appel, “On the potentials of passive, multistatic, low frequency radars to counter stealth and detect low flying targets,” in *Proc. of IEEE Radar Conf.*, May 2008, pp. 1443–1448.
- [12] C. Coleman, H. Yardley, and R. Watson, “A practical bistatic passive radar system for use with DAB and DRM illuminators,” in *Proc. of IEEE Radar Conf.*, May 2008, pp. 1514–1519.
- [13] C. R. Berger, S. Zhou, and P. Willett, “Signal extraction using compressed sensing for passive radar with OFDM signals,” in *Proc. of Intl. Conf. on Information Fusion*, Cologne, Germany, Jun. 2008.
- [14] C. R. Berger, S. Zhou, P. Willett, B. Demissie, and J. Heckenbach, “Compressed sensing for OFDM/MIMO radar,” in *Proc. of Asilomar Conf. on Signals, Systems, and Computers*, Monterey, CA, Oct. 2008.
- [15] M. Tobias and A. Lanterman, “Probability hypothesis density-based multitarget tracking with bistatic range and doppler observations,” *IEE Proc. Radar, Sonar & Navig.*, vol. 152, no. 3, pp. 195–205, Jun. 2005.
- [16] M. Daun and W. Koch, “Multistatic target tracking for non-cooperative illumination by DAB/DVB-T,” in *Proc. of IEEE Radar Conf.*, May 2008, pp. 1455–1460.
- [17] J. Li and P. Stoica, “MIMO radar with colocated antennas,” *IEEE Signal Processing Magazine*, vol. 24, no. 5, pp. 106–114, Sep. 2007.
- [18] A. M. Haimovich, R. S. Blum, and L. J. Cimini, “MIMO radar with widely separated antennas,” *IEEE Signal Processing Magazine*, vol. 25, no. 1, pp. 116 – 129, Jan. 2008.
- [19] S. Mallat and Z. Zhang, “Matching pursuits with time-frequency dictionaries,” *IEEE Trans. Signal Processing*, vol. 41, no. 12, pp. 3397–3415, Dec. 1993.
- [20] J. A. Tropp and A. C. Gilbert, “Signal recovery from random measurements via orthogonal matching pursuit,” *IEEE Trans. Inform. Theory*, vol. 53, no. 12, pp. 4655–4666, Dec. 2007.
- [21] E. Candes, J. Romberg, and T. Tao, “Robust uncertainty principles: exact signal reconstruction from highly incomplete frequency information,” *IEEE Trans. Inform. Theory*, vol. 52, no. 2, pp. 489–509, Feb. 2006.
- [22] D. Donoho, “Compressed sensing,” *IEEE Trans. Inform. Theory*, vol. 52, no. 4, pp. 1289–1306, Apr. 2006.
- [23] E. Candes and T. Tao, “Near-optimal signal recovery from random projections: Universal encoding strategies?” *IEEE Trans. Inform. Theory*, vol. 52, no. 12, pp. 5406–5425, Dec. 2006.
- [24] European Telecommunications Standards Institute, “Radio broadcasting systems; digital audio broadcasting (DAB) to mobile, portable and fixed receivers,” ETS 300 401, May 1997.
- [25] N. Levanon, *Radar Principles*. New York: J. Wiley & Sons, 1988.
- [26] H. Van Trees, *Optimum Array Processing*, 1st ed., ser. Detection, Estimation, and Modulation Theory (Part IV). New York: John Wiley & Sons, Inc., 2002.
- [27] T.-J. Shan, M. Wax, and T. Kailath, “On spatial smoothing for direction-of-arrival estimation of coherent signals,” *IEEE Trans. Signal Processing*, vol. 33, no. 4, pp. 806–811, Aug. 1985.
- [28] J. R. Magnus and H. Neudecker, “The commutation matrix: Some properties and applications,” *Ann. Statist.*, vol. 7, no. 2, pp. 381–394, 1979.
- [29] S.-J. Kim, K. Koh, M. Lustig, S. Boyd, and D. Gorinevsky, “An interior-point method for large-scale l_1 -regularized least squares,” *IEEE J. Select. Topics Signal Proc.*, vol. 1, no. 4, pp. 606–617, Dec. 2007.
- [30] M. A. T. Figueiredo, R. D. Nowak, and S. J. Wright, “Gradient projection for sparse reconstruction: Application to compressed sensing and other inverse problems,” *IEEE Trans. Signal Processing*, vol. 4, no. 1, pp. 586–597, Dec. 2007.

PLACE
PHOTO
HERE

Christian R. Berger (S’05–M’09) was born in Heidelberg, Germany, on September 12, 1979. He received the Dipl.-Ing. degree from the Universität Karlsruhe (TH), Karlsruhe, Germany in 2005, and the Ph.D. degree from the University of Connecticut, Storrs in 2009, both in electrical engineering.

In the summer of 2006, he was as a visiting scientist at the Sensor Networks and Data Fusion Department of the FGAN Research Institute, Wachtberg, Germany. He is currently a post-doctoral researcher at the Department of Electrical and Computer Engineering, Carnegie Mellon University, Pittsburgh, USA. His research interests lie in the areas of communications and signal processing, including distributed estimation in wireless sensor networks, wireless positioning and synchronization, underwater acoustic communications and networking.

Dr. Berger has served as a reviewer for the IEEE Transactions on Signal Processing, Wireless Communications, Vehicular Technology, and Aerospace and Electronic Systems. In 2008 he was member of the technical program committee and session chair for the 11th International Conference on Information Fusion in Cologne, Germany.

PLACE
PHOTO
HERE

Bruno Demissie (birth name Hüpper) received the diploma degree from the Ruhr-University-Bochum, Germany and the Dr. rer. nat. degree from the Carl-von-Ossietzky university in Oldenburg, Germany, both in theoretical physics, in 1994 and 1997 respectively. Afterwards, he had a post-doctoral researcher position at the Phillips-University in Marburg, Germany. From 1998 until 2000 he was at the Weizmann Institute of Science in Rehovot, Israel, as a MINERVA fellow. Since 2000 he has been working at the Fraunhofer Institute for Communications, In-

formation Processing and Ergonomics, formerly Research Establishment for Applied Sciences (FGAN), in Wachtberg, Germany. His research interests are on passive localization as well as blind equalization and system identification.

PLACE
PHOTO
HERE

Jörg Heckenbach was born in Ahrweiler, Germany, in 1967. He received the Dipl.-Ing. degree in electrical engineering in 1993 at RWTH Aachen University. Since 1994 he has worked as a Researcher at the Department of Passive Sensorsystems and Classification of the Fraunhofer Institute for High Frequency Physics and Radar Techniques FHR in Wachtberg, Germany. His research interests include Passive Coherent Location and High Performance Cluster.

PLACE
PHOTO
HERE

Shengli Zhou (M'03) received the B.S. degree in 1995 and the M.Sc. degree in 1998, from the University of Science and Technology of China (USTC), Hefei, both in electrical engineering and information science. He received his Ph.D. degree in electrical engineering from the University of Minnesota (UMN), Minneapolis, in 2002.

He has been an assistant professor with the Department of Electrical and Computer Engineering at the University of Connecticut (UConn), Storrs, 2003-2009, and now is an associate professor. He

holds a United Technologies Corporation (UTC) Professorship in Engineering Innovation, 2008-2011. His general research interests lie in the areas of wireless communications and signal processing. His recent focus is on underwater acoustic communications and networking.

Dr. Zhou has served as an associate editor for IEEE Transactions on Wireless Communications from Feb. 2005 to Jan. 2007, and is now an associate editor for IEEE Transactions on Signal Processing. He received the 2007 ONR Young Investigator award and the 2007 Presidential Early Career Award for Scientists and Engineers (PECASE).

PLACE
PHOTO
HERE

Peter Willett (F'03) received his B.A.Sc (Engineering Science) from the University of Toronto in 1982, and his PhD degree from Princeton University in 1986.

He has been a faculty member at the University of Connecticut ever since, and since 1998 has been a Professor. His primary areas of research have been statistical signal processing, detection, machine learning, data fusion and tracking. He has interests in and has published in the areas of change/abnormality detection, optical pattern recognition, communications and industrial/security condition monitoring.

Dr. Willett is editor-in-chief for IEEE Transactions on Aerospace and Electronic Systems, and until recently was associate editor for three active journals: IEEE Transactions on Aerospace and Electronic Systems (for Data Fusion and Target Tracking) and IEEE Transactions on Systems, Man, and Cybernetics, parts A and B. He is also associate editor for the IEEE AES Magazine, editor of the AES Magazines periodic Tutorial issues, associate editor for ISIFs electronic Journal of Advances in Information Fusion, and is a member of the editorial board of IEEE's Signal Processing Magazine. He has been a member of the IEEE AESS Board of Governors since 2003. He was General Co-Chair (with Stefano Coraluppi) for the 2006 ISIF/IEEE Fusion Conference in Florence, Italy, Program Co-Chair (with Eugene Santos) for the 2003 IEEE Conference on Systems, Man, and Cybernetics in Washington DC, and Program Co-Chair (with Pramod Varshney) for the 1999 Fusion Conference in Sunnyvale.